Journal of Materials Processing Technology 219 (2015) 155–163

Contents lists available at ScienceDirect

Journal of Materials Processing Technology

journal homepage: www.elsevier.com/locate/jmatprotec

Creep-age forming AA2219 plates with different stiffener designs and pre-form age conditions: Experimental and finite element studies

Aaron C.L. Lam[a], Zhusheng Shi[a,*], Haoliang Yang[b], Li Wan[c], Catrin M. Davies[a], Jianguo Lin[a], Shijie Zhou[c]

[a] Department of Mechanical Engineering, Imperial College London, SW7 2AZ, UK
[b] Beijing Institute of Astronautical Systems Engineering, Beijing 100076, PR China
[c] The Capital Aerospace Machinery Company, No. 2 Jingbei East Road, Feng Tai District, Beijing 100076, PR China

ARTICLE INFO

Article history:
Received 7 October 2014
Received in revised form 9 December 2014
Accepted 13 December 2014
Available online 24 December 2014

Keywords:
Creep-age forming
Aluminium alloy 2219
Integral airframe structures
Pre-form age condition
Stiffener design
Springback

ABSTRACT

Creep-age forming (CAF) is one of the relatively new forming techniques that has been proven viable for the production of extra-large integral airframe structures. However, experimental studies on forming stiffened structures under creep-ageing conditions remain scarce. In this work, 200 mm × 48 mm integrally stiffened plates of aluminium alloy 2219 have been formed on an end clamp device that has a bending radius of 156 mm and creep-aged at 175 °C for 18 h. Three different stiffener designs, namely the beam stiffened, waffle and isogrid plates, are tested alongside the flat plates. Utilisation of PTFE pocket fillers and intermediate sheets to reinforce and protect stiffeners during forming operation is found effective as demonstrated by the defect-free formed parts with smooth curvature. Springback of the plates ranged from 12.2 to 15.7% in the experimental studies for different stiffener designs. Using the CAF material constants determined for this alloy, corresponding finite element models have been developed and experimentally validated using the measured profiles of the creep-age formed plates. Up to 6.3% difference in springback is observed when forming workpieces with different pre-form age condition alone.

1. Introduction

In the late 20th century, the National Aeronautics and Space Administration (NASA) launched a programme aimed to organise initiatives towards a technology of interest – the integral airframe structures (IAS). IAS was an alternative approach to the traditional riveted skin-stringer aircraft construction, such that for an IAS panel, skin and stringers became an integrated single piece structure (Fig. 1). As manufacturing technology advanced, high-speed machining of structure of aluminium plate became more economically available and increased attention has been brought to the IAS programme as a result (Munroe et al., 2000).

In a cost assessment conducted by Boeing (Chicago, IL, USA), an integral panel was found to have achieved 91% reduction in the number of parts and 58% reduction in manufacturing cost compared to a standard built-up fuselage panel from a Boeing 747. Crack tests also revealed a remarkable three times higher crack growth life and 3% increase in residual strength in the IAS panel (Munroe et al., 2000). Despite the advantages of IAS, with stiffeners integrated to the primary structure, conventional forming technique such as roll forming and bump forming were soon found to be inadequate (Munroe et al., 2000).

Creep-age forming (CAF) is one of the few processing techniques that has been proven viable by researchers for the production of extra-large IAS panels (Eberl et al., 2008). These are panels that have typical dimensions of 33 m in length, 2.7 m in width and thickness that can vary from 2 to 32 mm within the same component, such as those seen in the wing skin of modern aircrafts (Levers, 2004). Due to the small curvature required for forming aircraft wing panel components, plastic strain is usually not present in the panel during the loading phase of a CAF process. Forming stress is partially relieved in the creep-ageing phase whilst the remaining is relieved as the panel component returns towards its original shape upon unloading – a phenomenon known as springback. Springback is a common problem seen in sheet metal forming processes and is particularly important in CAF where springback can reach over 80% (Ho et al., 2004a).

Springback compensation is a substantial topic by itself but in all cases, reliable indicators of springback must first be determined before effective springback compensation methods can be

* Corresponding author. Tel.: +44 2075947130.
E-mail address: zhusheng.shi@imperial.ac.uk (Z. Shi).

http://dx.doi.org/10.1016/j.jmatprotec.2014.12.012

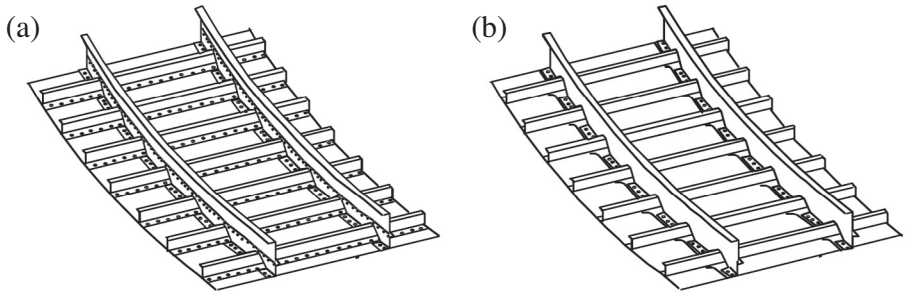

Fig. 1. A comparison of (a) a conventional built-up structure and (b) an advanced integrally stiffened structure (Munroe et al., 2000).

established. Research and development of CAF-specific constitutive equations have started soon after the first introduction of CAF in 1989 (Holman, 1989). Peddieson and Buchanan (1990) developed one of the first CAF-specific models based on the Euler–Bernoullie beam theory in conjunction with a linear viscoelastic model. An experimentally validated model was later developed by Sallah et al. (1991) who utilised modified Maxwell and Walker/Wilson models for describing the stress relaxation of an Euler–Bernoulli beam under CAF conditions.

Based on the creep damage constitutive equations developed by Kowalewski et al. (1994a,b), Ho et al. (2004a) developed a set of creep-ageing constitutive equations and implemented them into a finite element (FE) solver to simulate the creep forming of thick aluminium flat sheets. Ho et al. (2004b) further introduced precipitate nucleation and growth into unified creep-ageing constitutive equations and Zhan et al. (2011a) proposed a new set of unified creep-ageing constitutive equations for the modelling of precipitate nucleation, growth, dislocation density and their effects on the creep deformation and the mechanical properties of creep-age formed plates.

To date, research in CAF has mostly been conducted on flat panel components and CAF-specific literature on stiffened structures remains scarce. One of which is due to Guines et al. (2008) who numerically modelled the CAF of an integrally stiffened panel with single curvature bending. Hardening, thermal softening, and stress relaxation effects of the stiffened panel have been modelled. The authors suggested future work to include experimental studies on CAF stiffened structures. More recently, Inforzato et al. (2012) adapted a semi-empirical model for CAF springback estimation of an aluminium alloy 7475, or AA7475, stiffened panel. The simplified model, which is based on classical plate bending theory combined with the concept of equivalent height, requires calibration using experimentally measured deflections. A 600 mm × 300 mm AA7475 plate was flat machined down from a 50.8 mm thick plate to an integrally stiffened panel with a 5 mm thick base and eleven height-varying blade stiffeners. CAF of the stiffened component was carried out using a vacuum bagging technique for load application. The calculated radii of the creep-age formed part ranged from 820 to 2600 mm and the calibrated model was found to be able to provide estimations to an accuracy of within ±1.3% of springback.

This paper investigates experimentally and numerically the mechanics of creep-age forming AA2219 plates with three different types of integral stiffener designs, namely the beam stiffened, waffle and isogrid plates, alongside the flat plates. A novel technique that makes use of pocket fillers and intermediate sheets for forming stiffened plates is conceived and put to use. AA2219 material constants for CAF have been determined for this study and are implemented into the corresponding FE models. Accuracy of the FE models is established using the experimental results and further simulations are performed using the validated models to study the effect of pre-form age conditions on springback in CAF.

2. Materials and method

2.1. Equipment

An end clamp device was manufactured to the design and dimensions shown in Fig. 2. The complete setup, which consists of the end clamp device, intermediate sheets, pocket fillers (not illustrated) and workpiece, is placed on an Instron (Norwood, MA, USA) 5585H advanced materials testing system where loading and unloading take place.

Heating during the creep-ageing phase is supplied by a 1200 °C laboratory chamber furnace manufactured by the Elite Thermal Systems (Leicestershire, England, UK). Heat treatment cycle of the creep-ageing phase is programmed and controlled via the Eurotherm (Ashburn, VA, USA) 2408 programmer and 2216 over-temperature controller respectively. Coordinate graph papers were used to visualise the shape of each formed part's profile.

2.2. Unified creep-ageing constitutive equations

The following set of constitutive equations proposed by Zhan et al. (2011a) is employed to model the creep deformation and ageing kinetics of the AA2219 used in this study.

$$\dot{\varepsilon}_e^{cr} = A_1 \sinh\{B_1[\sigma_e(1-\bar{\rho}_d) - k_{\varepsilon c}\sigma_y]\} \quad (1)$$

$$\dot{\sigma}_{age} = C_a \dot{\bar{r}}_p^{m_1}(1-\bar{r}_p) \quad (2)$$

$$\dot{\sigma}_{sol} = C_s \dot{\bar{r}}_p^{m_2}(\bar{r}_p - 1) \quad (3)$$

$$\dot{\sigma}_{dis} = A_2 \cdot n_d \cdot \bar{\rho}_d^{n_d-1}\dot{\bar{\rho}}_d \quad (4)$$

$$\sigma_y = \sigma_{sol} + \sqrt{\sigma_{age}^2 + \sigma_{dis}^2} \quad (5)$$

$$\dot{\bar{r}}_p = C_r(Q_r - \bar{r}_p)^{m_3}(1 + \gamma_r \bar{\rho}_d^{m_4}) \quad (6)$$

$$\dot{\bar{\rho}}_d = A_3(1-\bar{\rho}_d)\dot{\varepsilon}_e^{cr} - C_\rho \bar{\rho}_d^{m_5} \quad (7)$$

where A_1, B_1, $k_{\varepsilon c}$, C_a, m_1, C_s, m_2, A_2, n_d, C_r, Q_r, m_3, γ_r, m_4, A_3, C_ρ, m_5 are material constants in Eqs. (1)–(7). Equivalent rate of creep strain ($\dot{\varepsilon}_e^{cr}$) is a function of normalised dislocation density ($\bar{\rho}_d$), von Mises equivalent stress (σ_e) and the material's yield strength (σ_y) as described by Eq. (1). $\bar{\rho}_d = (\rho - \rho_i)/\rho_m$ where ρ_i and ρ_m are respectively the dislocation density of the virgin material and

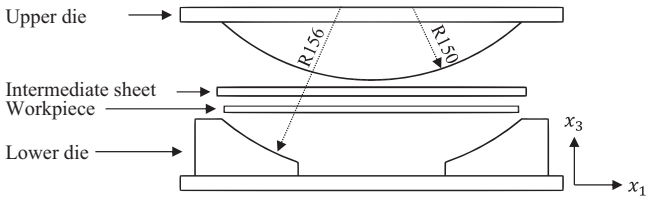

Fig. 2. Schematic of the experimental setup (units in mm).

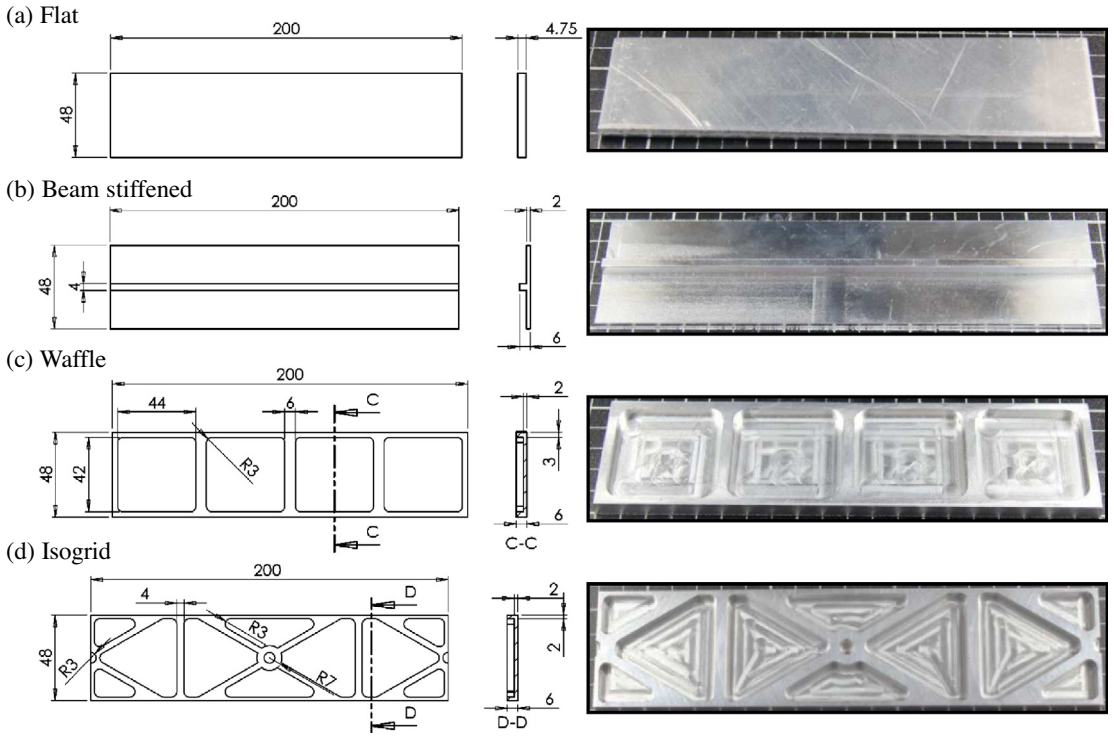

Fig. 3. Dimensions of the plate designs (units in mm). Certain key dimensions of the isogrid plates are not shown with intent.

Table 1
Chemical compositions of AA2219 (wt%).

Cu	Mn	Si	Fe	Ti	Cr	Al
6.3	0.3	0.2	0.3	0.06	0.18	Bal.

the maximum (saturated) dislocation density that the material could have. Thus ρ varies from ρ_i to ρ_m and $\bar{\rho}_d$ varies from 0 (initial) to 1 (saturation), assuming $\rho_i \ll \rho_m$. During CAF, the material is strengthened due to ageing (σ_{age}), solute hardening (σ_{sol}) and work (dislocation) hardening (σ_{dis}). The kinetics of these hardening mechanisms are described by Eqs. (2)–(4) respectively, and each of their contribution to σ_y is described by Eq. (5). Effects of σ_{age} and σ_{sol} on creep deformation are taken into account by $\bar{\rho}_d$ and the normalised radius of precipitates $\bar{r}_p$. $\bar{r}_p = r/r_c$ where r and r_c are the current and peak-aged precipitate size respectively. $0 \le \bar{r}_p < 1$ indicates under-ageing, $\bar{r}_p = 1$ indicates peak-ageing, and the material is over-aged when $\bar{r}_p > 1$. More detailed description of the equations can be referred to Zhan et al. (2011a).

2.3. Materials

Experimental investigations on the mechanical properties of AA2219 have been conducted (Yang, 2013), where coupons of composition shown in Table 1 have been tested for their basic mechanical properties and creep-ageing behaviour at 175 °C to be determined (as described by Eqs. (1)–(7)). A detailed test programme for this material investigation can be referred to Yang (2013) and the results are summarised in Tables 2 and 3.

Table 2
Basic mechanical properties of AA2219-T4 and -T87.

	E (GPa)	σ_y (MPa)	σ_{uts} (MPa)
T4 (naturally aged)	69.0	139.1	320.4
T87 (peak-aged)	72.2	297.3	420.6

Table 3
CAF material constants of AA2219 (175 °C, 18 h).

A_1	B_1	$k_{\varepsilon c}$	C_a	m_1	C_s	m_2	n_d	A_2
1.6E−10	0.101	0.08	50.1	0.42	15.0	0.85	0.9	520

C_r	Q_r	γ_r	m_3	m_4	A_3	C_ρ	m_5
0.032	1.76	2.7	1.6	2.1	35	0.318	1.01

Four workpiece designs as illustrated in Fig. 3 are supplied in the form of T87 (peak-aged) condition. Each workpiece is solution heat treated at 535 °C for 1 h and water quenched immediately prior to each test in order to prepare the material to T4 (naturally aged) condition.

AA2219 at its T4 condition is a relatively soft material when compared to the tooling steel of which the end clamp device is made. Excessive contact loads being applied directly onto the stiffeners can damage the component during loading. A novel forming technique is conceived which makes use of pocket fillers and intermediate sheets to minimise the direct contact force experienced by the stiffeners. Fig. 4 illustrates a waffle plate with pocket fillers

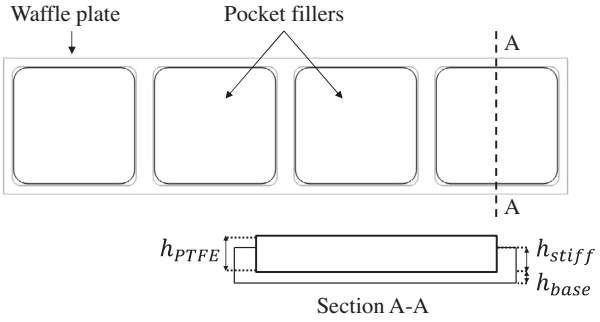

Fig. 4. Schematic of a waffle plate with its pocket fillers.

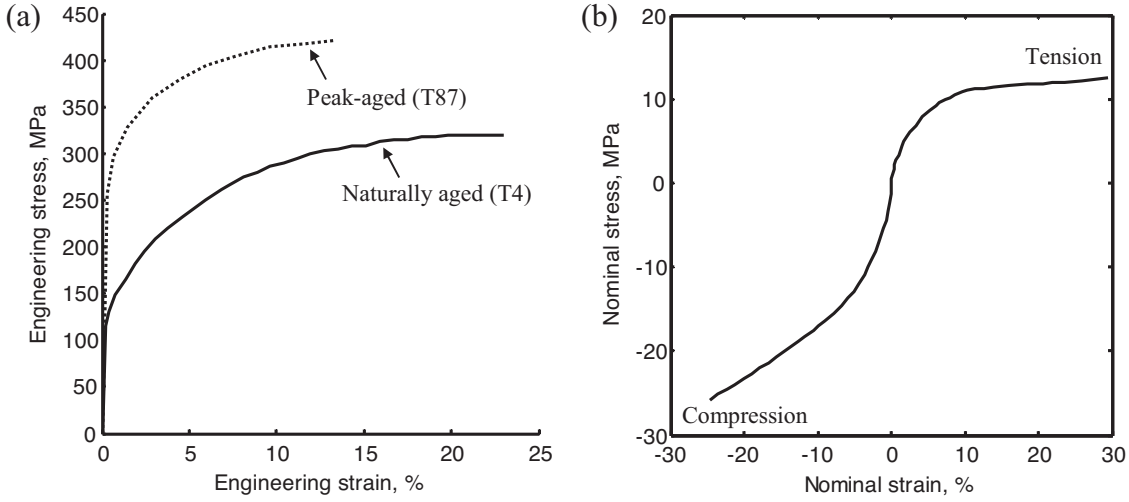

Fig. 5. Stress–strain behaviours of (a) AA2219 and (b) PTFE.

sitting inside its machined pockets. Thickness of the pocket fillers (h_{PTFE}) is slightly larger than the height of the stiffeners (h_{stiff}) and the pocket fillers therefore protrude slightly from the top surface of the plate. Top surface of the pocket fillers are then topped with an intermediate sheet (not illustrated), which sits between the top die and the pocket fillers.

Teadit (Teadit International, Kufstein, Austria) 24SH PTFE, which has an operating temperature range of −240 to +270 °C, is chosen to be the intermediate sheet and pocket filler material. This is due to (i) its rubber-like behaviour which can transmit and distribute the applied loads back into the machined pockets and (ii) its ability to withstand elevated temperature at a relatively low cost compared to high temperature polymers. The minimum h_{PTFE} required is first chosen based on FE analyses considering the stress–strain behaviours of the materials (Fig. 5) with a focus on minimising the loads experienced by stiffeners during loading. h_{PTFE} = 6 mm is selected for the experiments which is a compromise between the analysis result and the thickness available from suppliers. Table 4 summarises the material type and dimensions of the intermediate sheet, pocket fillers and workpiece.

Table 4
Material type and dimensions of the intermediate sheet, pocket fillers and workpiece.

	Material	Thickness (mm)	Length × width (mm)
Intermediate sheet	PTFE	6	210 × 50
Pocket fillers	PTFE	6	Var. (Fig. 3)
Workpiece	AA2219	Var. (Fig. 3)	200 × 48

2.4. Experimental procedure

A typical CAF process can be split into three main steps: loading, creep-ageing, and unloading (Zhan et al., 2011b). Before the CAF experiments begin, pocket fillers are prepared for the waffle and

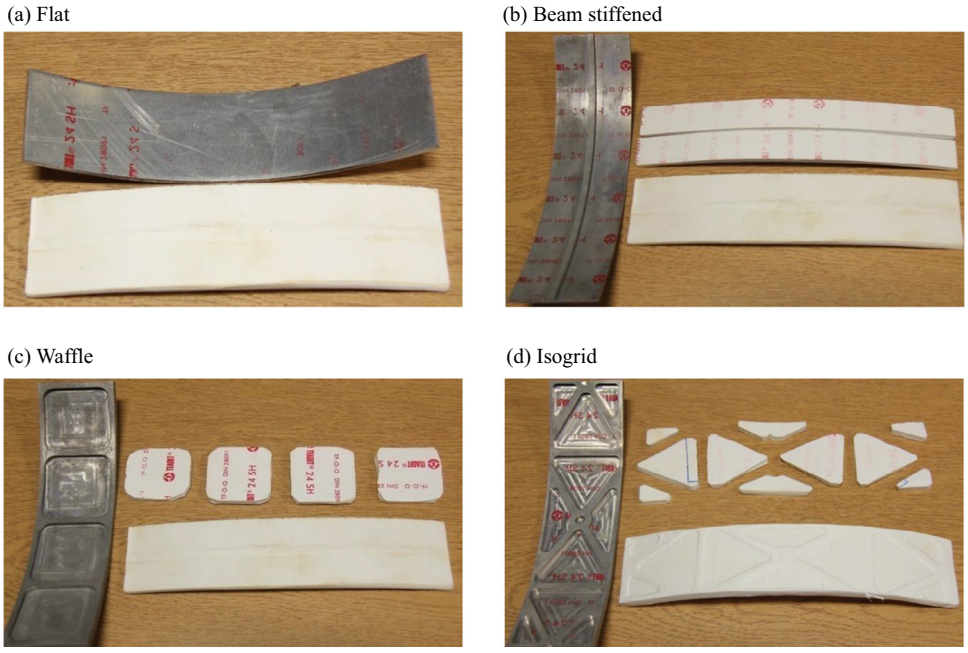

Fig. 6. (a) The flat and (b–d) stiffened plates and their corresponding pocket fillers and intermediate sheets.

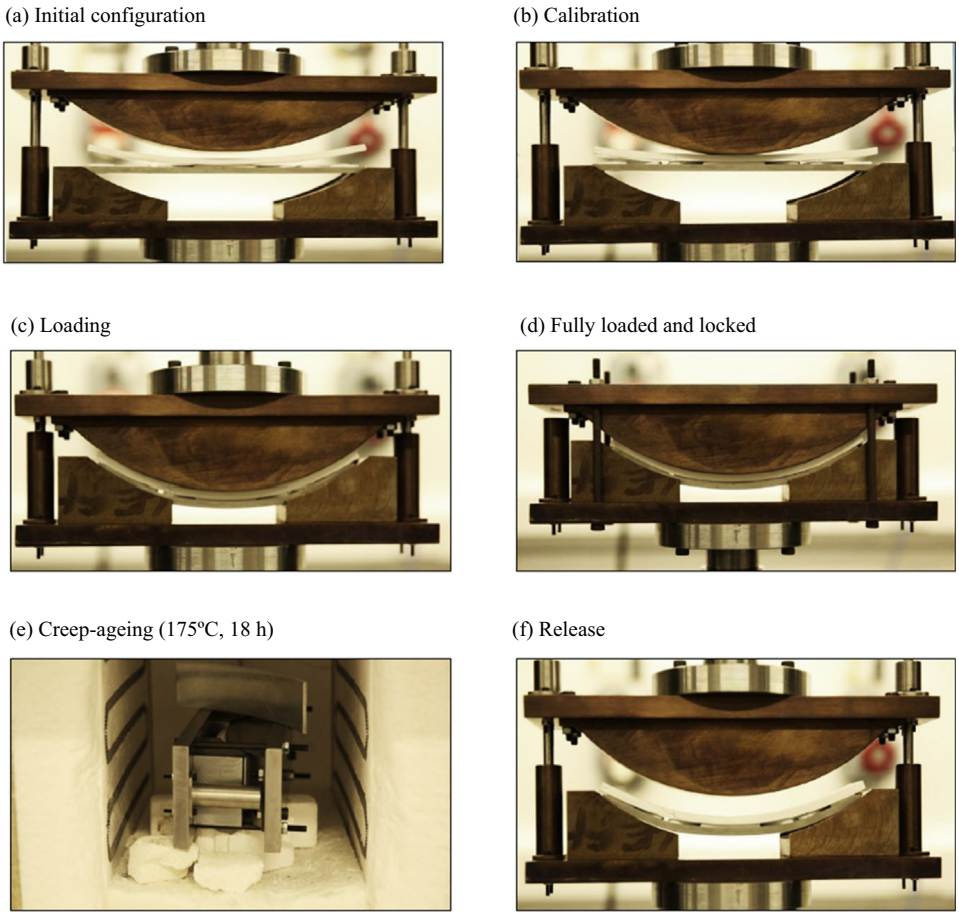

Fig. 7. Different stages of a CAF experiment.

isogrid plates by trimming out the shape of the machined pockets from the PTFE sheets (Fig. 6).

In the loading stage, a workpiece is first placed on the two end clamps. For the waffle and isogrid type workpiece, pocket fillers are also placed inside the machined pockets. The workpiece is then aligned to the centre of the forming tool with the aid of visual markings. Once aligned, another 6 mm thick PTFE sheet, which has in-plane dimensions that are slightly larger than that of the workpiece, is placed on top of the pocket fillers that sit inside the machined pockets and protrude from the stiffeners (Fig. 7(a)).

With the testing machine set to be in displacement control mode, the crosshead, which applies loading onto the upper die, is lowered. This is continued until an obvious positive change in loading is observed; such change indicates a compressive force is beginning to be transmitted and therefore the upper die is now in actual contact with the intermediate sheet (Fig. 7(b)).

The displacement and load are then zeroed and the crosshead is allowed to travel down to achieve target distance (Fig. 7(c)). Four locking bolts are then applied to tighten the upper die of the end clamp device in order to hold the workpiece in place. A negligible loading value displayed on the status console can confirm the complete transfer of loading from the crosshead to the four bolts (Fig. 7(d)).

In its loaded configuration, the complete tooling is removed from the testing machine and put into a furnace. The furnace is programmed and controlled to provide a constant temperature of 175 °C for 18 h to allow creep-ageing to take place (Fig. 7(e)). After 18 h, the furnace is ventilated for up to 3 h to allow the apparatus to return to room temperature. Unloading takes place with the aid of the testing machine; the locking bolts are removed from the cooled apparatus, the top die is raised and the workpiece is allowed to springback (Fig. 7(f)).

In order to record their shape profile, each creep-age formed part is placed and aligned on a coordinate graph paper. The shape of the part's surface is marked on the paper, starting from the line of symmetry and working towards its ends at 10 mm intervals. Subsequent measurements and calculations are made and the data is transferred to a computer, where each shape is averaged for both sides of the symmetry and plotted. A springback factor S given by

$$S = \left(1 - \frac{\delta_f}{\delta_0}\right) \times 100\% \tag{8}$$

is used to evaluate the springback of each formed plate. δ_0 and δ_f denote the plate's initial and final maximum vertical deflection, which in this case is also the centre deflection of the workpiece with $\delta_0 = 28.6$ mm. Experiments were repeated on two flat, two waffle, five beam stiffened and over ten isogrid plates, and the error of springback is within ±5%.

3. FE process simulations

FE process simulations are conducted using Abaqus 6.11 (Dassault Systèmes Simulia, Providence, RI, USA). Half models are used which best compromise between ease of analyses and computational cost. Geometric models of the upper and lower dies are first generated using SolidWorks 2012 Education Edition (Dassault Systèmes SolidWorks, Waltham, MA, USA) as IGES files v5.3 and imported into Abaqus as 3D discrete rigid solid. 'Create shell: from solid' feature is used to convert the surfaces

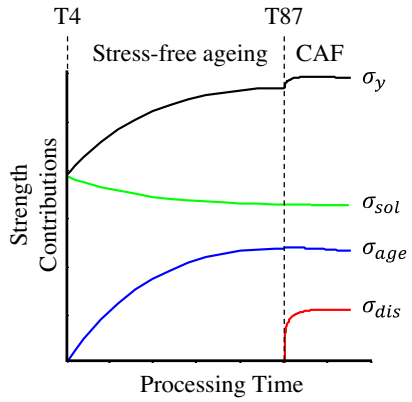

Fig. 8. A typical creep-age hardening trace showing how the T87 condition is numerically achieved.

of the solid dies into rigid shell elements R3D4. PTFE sheets are modelled as 3D deformable solid and discretised using eight-node linear brick elements C3D8RH. Reduced integration and hybrid formulation options are activated as indicated by the letters 'R' and 'H'. Reduced integration is activated to avoid shear and membrane locking whilst hybrid formulation is commonly used to model rubber-like material behaviour for incompressible ($\upsilon = 0.5$) or near incompressible ($\upsilon > 0.475$) materials (Abaqus, 2011). Workpieces are modelled as 3D deformable shells and discretised using four-node linear shell elements S4R, again with reduced integration activated. For the beam stiffened, waffle and isogrid plates, extra shell elements are created and positioned according to the designs in Fig. 3. The instances are then merged to create a single stiffened plate model with the base plate and stiffeners assigned to different sections, allowing different thickness values to be assigned.

The basic mechanical properties shown in Table 2 and Fig. 5(a) are assigned for the AA2219-T4 and -T87 conditions. Creep-ageing behaviour (Eqs. (1)–(7)) is implemented via the user-defined subroutine CREEP with 5 solution-dependent state variables and the material constants in Table 3 are used. PTFE is modelled as an isotropic hyperelastic material using Mooney–Rivlin strain energy potential and the uniaxial test data presented in Fig. 5(b).

Under typical CAF conditions where deformation of a material remains elastic (below 0.2% strain), residual stress induced by the heat treatment of thick material prior to CAF (such as quenching) may cause notable effects on springback. In the present work, thin plates are studied and the plates are loaded to a maximum

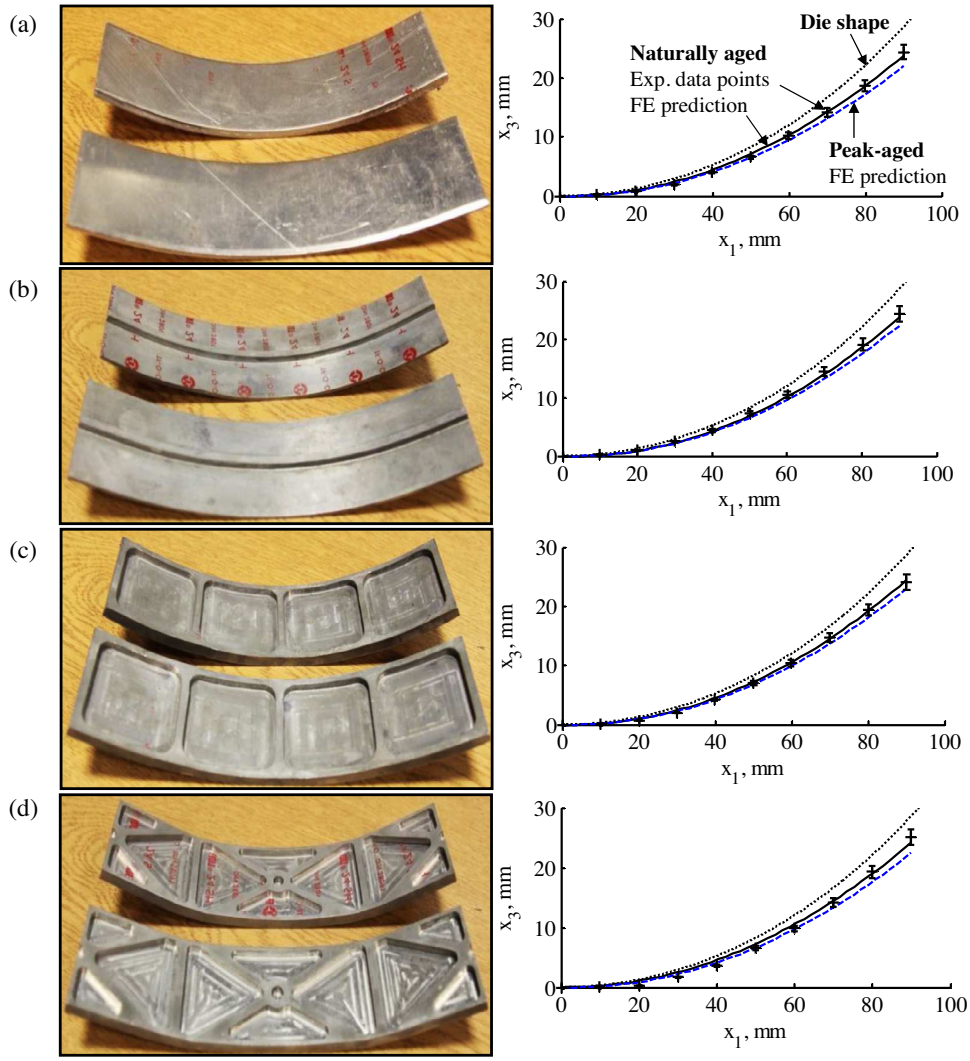

Fig. 9. Left: images of the creep-age formed (a) flat, (b) beam stiffened, (c) waffle, and (d) isogrid plates. Right: measured ("+" markers with error bars in the x_3 direction) and predicted (solid line for the T4 and dashed line for the T87 pre-form age conditions) profiles of the plates.

strain of approximately 5%, which indicates a significant amount of plastic deformation. In this case, when fully loaded, the total stress will be similar with or without residual stress according to the stress–strain behaviour of the material (Fig. 5(a)). The significant plastic deformation dwarfs the effects of residual stress on springback and therefore residual stress is not included in the simulations.

A four-step analysis is conducted – firstly, symmetric boundary conditions are defined and allowed to propagate throughout the entire simulation. Secondly, u_3 loading conditions are applied to the upper die with a ramp control over a static loading period of 10 h. Thirdly, the tool and workpiece are held in their loaded configurations for 18 h in a visco step for creep-ageing to take place. Finally, the upper die is released with u_3 reverted back to its original position with a 10 h ramp control as springback of the workpiece occurs.

As mentioned, the effect of pre-form age conditions on springback in CAF is also investigated through simulations. Since the CAF material constants have been obtained for an AA2219 with T4 starting condition, an extra stress-free ageing step was introduced to the analysis, after the initiation and before the loading step, in order to model the behaviour of T87 in CAF. Fig. 8 shows how the T87 condition was numerically achieved before CAF took place from the perspective of a material's creep-age hardening history.

4. Experimental and computational results

4.1. On CAF operation

Fig. 9 shows the profiles of the simulated formed part shape for both the naturally aged (T4) and peak-aged (T87) workpieces. Die shape and the recorded profile of the experimentally formed plates are also illustrated for direct comparison.

AA2219-T4 is a relatively soft material when compared to the tooling material and that defects can easily be introduced during CAF operations. This problem can get worse when forming stiffened structures where high load concentration is seen on the stiffeners that protrude from the base plate. The creep-age formed plates in this study all exhibit a smooth curvature and that inspection of the formed plates concluded no defects on all parts including their stiffeners (Fig. 9). The experiments confirm that with the use of pocket fillers and intermediate sheet to reinforce and protect stiffeners, integrally stiffened plates of different stiffener designs can be formed defect-free.

Table 5
A summary of the experimentally measured and predicted springback.

		T4 experiment	T4 prediction	T87 prediction
δ_f (mm)	Flat	24.3	23.8	22.0
	Beam stiffened	24.4	23.8	22.4
	Waffle	24.1	24.4	23.0
	Isogrid	25.1	24.2	22.4
S (%)	Flat	15.0	16.8	23.1
	Beam stiffened	14.7	16.8	21.7
	Waffle	15.7	14.7	19.6
	Isogrid	12.2	15.4	21.7

4.2. On pre-form age condition

Table 5 summarises the values of final centre deflection (δ_f) and the calculated springback factor (S) for each plate. Validity of the developed FE models are confirmed by comparing the predicted formed part shape with that recorded from the experiments for the T4 plates (Fig. 9). The developed FE models predicted final deflections to an accuracy of ±0.9 mm, or ±3.2% of springback. Profiles of the formed plates at T4 and T87 conditions in Fig. 9 show that the T87 plates generally have larger springback, and their profiles are close to the boundaries of the measured T4 profiles when the experimental error of ±5% is considered.

CAF is a forming process that utilises stress relaxation (due to creep) of a material, and the amount of stress that is relaxed has a nonlinear but proportional relationship with the magnitude of the current σ_e in the material. This means that higher stress state in the material will translate to more stress being relaxed during the CAF process. As die shape is typically fixed in CAF, the amount of strain will be identical between workpieces. Referring back to the

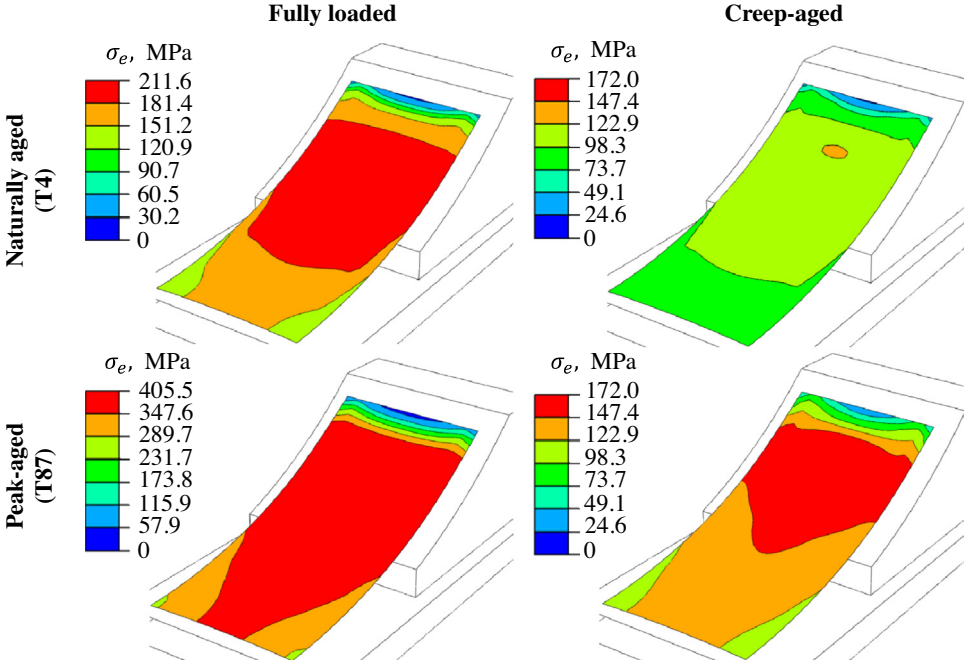

Fig. 10. A comparison of the amount of stress relaxation occurred in the T4 and T87 flat plates.

alloy in the present study (Fig. 5(a)), one may therefore expect to observe more stress relaxation to occur in the T87 plates.

Fig. 10 compares the amount of stress relaxation over the creep-ageing step for the T4 and T87 flat plates. When fully loaded, the T4 plate has a peak σ_e of 211.6 MPa; this is reduced to 123.6 MPa after 18 h of creep-ageing, equivalent to a reduction of 41.6%. At its peak-aged condition, both the yield and ultimate tensile strengths of the material are higher (Fig. 5). Therefore, when given the same amount of strain, σ_e of the T87 plate peaks at 405.5 MPa and is reduced to 171.2 MPa after creep-ageing – this is equivalent to a stress relaxation of 57.8% which in fact is much greater than that of the T4 plate.

More stress relaxation does not always translate to more permanent deformation being retained in a creep-age formed part. Stress relaxation that occurred in the T4 and T87 flat plates are 88.0 and 234.3 MPa respectively, which means the amount of stress relaxed in the T87 plate is 2.7 times greater. However, as the T87 plate is much stronger, the maximum ε_e^{cr} in the formed T87 plate remains smaller than that of the formed T4 plate. Greater springback is therefore observed in the T87 than in the T4 plates (Fig. 9). In the present study, predicted springback of components with different pre-form age condition alone (T4 vs. T87) varied up to 6.3% (Table 5).

4.3. On stiffener design

Fig. 11 shows the von Mises equivalent stress (σ_e) distributions captured at the end of each stage of the CAF process for the four plate designs, and their corresponding changes in peak σ_e are summarised in Table 6.

Springback in the experimental study ranged from 12.2% on the isogrid plate to 15.7% on the waffle plate. This is much lower than the 50–70% springback recorded by Adachi et al. (2004) due to the significant amount of plastic deformation that is involved in this study. Despite all the tests being carried out on the same tool (hence die shape) and same workpiece material, σ_e distributions in a workpiece throughout the entire CAF process can be vastly different depending on the stiffener design (Fig. 11). In some cases, maximum stress may occur on the stiffeners and cannot be seen from the view of the field plots in Fig. 11. A common feature amongst stiffener designs in this study is that peak σ_e is observed in the area where the workpieces are in contact with the end clamp. Since ε_e^{cr} is a function of σ_e (Eq. (1)), this indicates that die design may have an important influence on different aspects of creep-age formed parts, which include springback and the resulting mechanical properties. Similar conclusions were also drawn by Yang et al. (2013), who conducted a detailed examination on the effect of tooling designs on springback in CAF.

When bending stiffeners are present (as opposed to stiffeners in the non-bending direction), highest σ_e are found within and around them. The presence of bending stiffeners could therefore be seen acting as stress shields for the base plates, taking up a greater proportion of ε_e^{cr} during CAF. This may indicate that bending stiffeners are responsible for holding up most of the final shape of the formed plates, and such interpretation can be supported by the ε_e^{cr} plots in

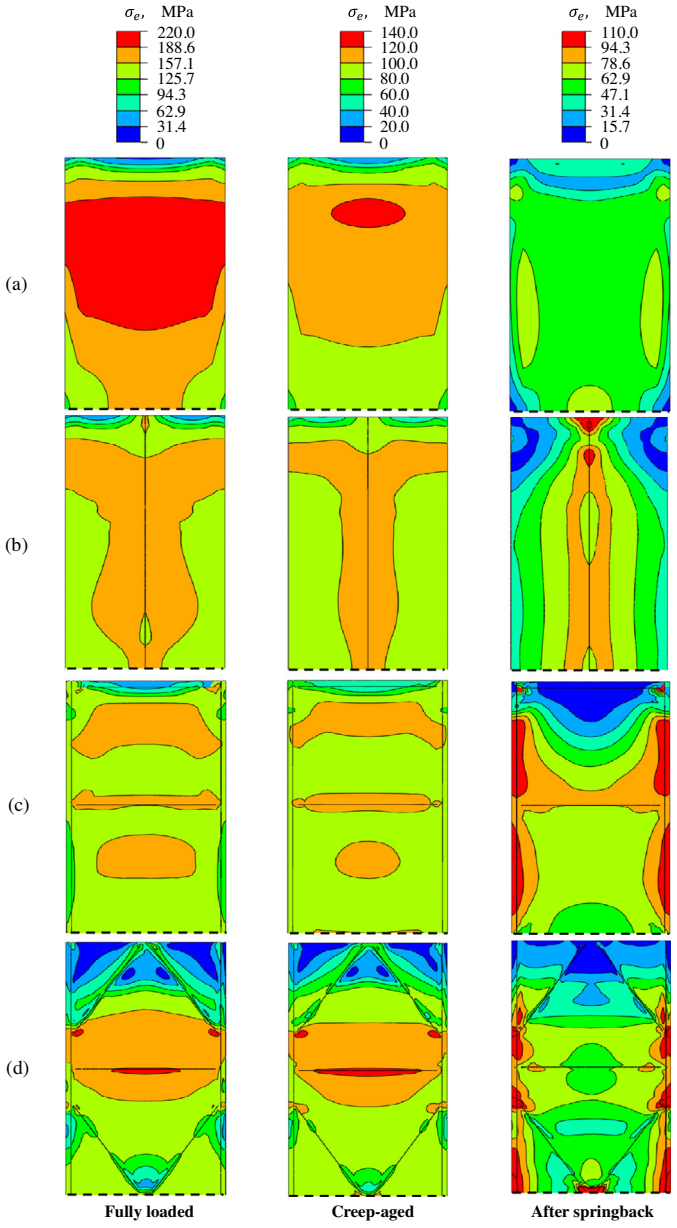

Fig. 11. Von Mises equivalent stress distributions on the base plate of the naturally aged (a) flat, (b) beam stiffened, (c) waffle, and (d) isogrid plates in CAF. The line of symmetry of each half model is indicated by the dashed line at the bottom.

Fig. 12 which illustrates the ε_e^{cr} distributions of the naturally aged plates. In Fig. 12, most of the ε_e^{cr} can be seen accumulated within and near the stiffeners, and that ε_e^{cr} are significantly lower in the area away from the stiffeners. In some cases, ε_e^{cr} are close to zero in certain regions of the base plate.

Table 6
Changes in peak σ_e during CAF of the stiffened T4 plates.

	Peak σ_e (MPa)			Relaxed σ_e	
	Fully loaded	After 18 h of creep-ageing	After springback	MPa	%
Flat	211.6	123.6	77.4	88.0	41.6
Beam stiffened	232.3	127.1	129.2	105.2	45.3
Waffle	233.6	132.2	156.4	101.4	43.4
Isogrid	274.9	169.1	216.0	105.8	38.5

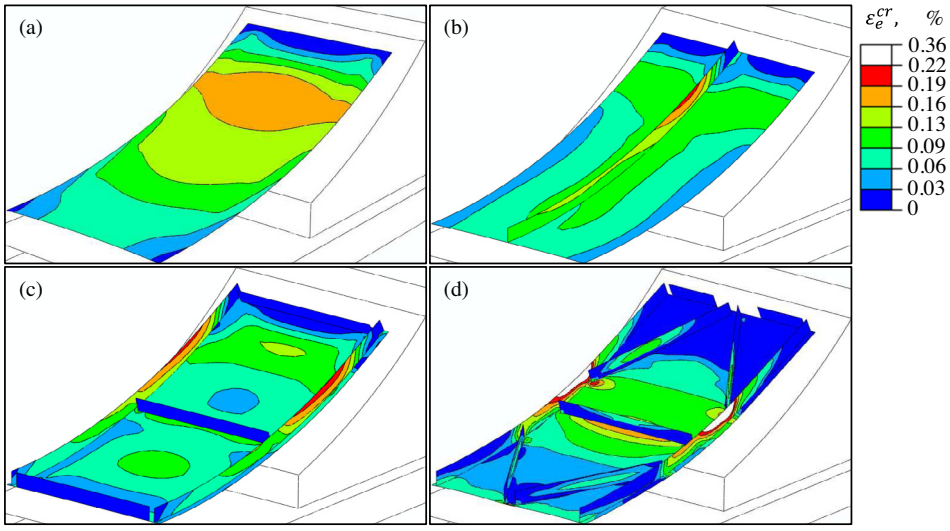

Fig. 12. Final equivalent creep strain distributions of the naturally aged (a) flat, (b) beam stiffened, (c) waffle, and (d) isogrid plates.

5. Conclusions

Mechanics of the creep-age forming of aluminium alloy 2219 integrally stiffened plates were experimentally studied on an end clamp device. Corresponding finite element models were developed for plates with different stiffener design and the results agree well with experimentally measured profiles of the creep-age formed plates. The following conclusions can be drawn from this study:

- A novel forming technique, which makes use of PTFE pocket fillers and intermediate sheets to reinforce and protect stiffeners during creep-age forming, can be used to produce defect-free formed parts with smooth curvature.
- Plastic deformation was reached under the loading condition studied, resulting in the low springback (around 15%) measured in the naturally aged plates.
- Pre-form age condition affects not only the peak σ_e of the plates during creep-age forming operations, but also their springback. For the flat plates in this study, maximum σ_e was 405.5 MPa for the peak-aged condition compared with 211.6 MPa for the naturally aged condition. The amount of stress relaxation in the stronger peak-aged plates was 2.7 times that in the naturally aged plates, but the peak-aged plates had up to 6.3% more springback than the naturally aged plates.
- When bending stiffeners are present, highest σ_e is more likely to occur within and around them. Bending stiffeners may therefore be seen as a form of stress shields for the base plates and take up a greater proportion of the creep strain in creep-age forming.

Acknowledgements

Financial support from International Science and Technology Cooperation Programme of China (Grant No. 2012DFA70430) is greatly appreciated. Support was also received from the Major State Basic Research Programme of China (973 Programme) (Grant No. 2014CB046602).

References

Abaqus, 2011. Abaqus 6.11 Theory Manual. Dassault Systèmes Simulia, Providence, RI, USA.
Adachi, T., Kimura, S., Nagayama, T., Takehisa, H., Shimanuki, M., 2004. Age forming technology for aircraft wing skin. Mater. Forum. 28, 202–207.
Eberl, F., Gardiner, S., Campanile, G., Surdon, G., Venmans, M., Prangnell, P., 2008. Ageformable panels for commercial aircraft. Proc. Inst. Mech. Eng. Part G: J. Aerosp. Eng. 222 (6), 873–886.
Guines, D., Gavrus, A., Ragneau, E., 2008. Numerical modeling of integrally stiffened structures forming from creep age forming technique. Int. J. Mater. Form. 10, 1071–1074.
Ho, K.C., Lin, J., Dean, T.A., 2004a. Modelling of springback in creep forming thick aluminum sheets. Int. J. Plast. 20 (4–5), 733–751.
Ho, K.C., Lin, J., Dean, T.A., 2004b. Constitutive modelling of primary creep for age forming an aluminium alloy. J. Mater. Process. Technol. 153–154, 122–127.
Holman, M.C., 1989. Autoclave age forming large aluminum aircraft panels. J. Mech. Work. Technol. 20, 477–488.
Inforzato, D.J., Costa Jr., P.R., Fernandez, F.F., Travessa, D.N., 2012. Creep-age forming of AA7475 aluminum panels for aircraft lower wing skin application. Mater. Res. 15 (4), 596–602.
Kowalewski, Z.L., Hayhurst, D.R., Dyson, B.F., 1994a. Mechanisms-based creep constitutive equations for an aluminium alloy. J. Strain Anal. Eng. Des. 29 (4), 309–316.
Kowalewski, Z.L., Lin, J., Hayhurst, D.R., 1994b. Experimental and theoretical evaluation of a high-accuracy uni-axial creep testpiece with slit extensometer ridges. Int. J. Mech. Sci. 36 (8), 751–769.
Levers, A., 2004. Aircraft Component Manufacturing Tool and Method, EP 1581357 B1 (Patent).
Munroe, J., Wilkins, K., Gruber, M., 2000. Integral Airframe Structures (IAS) - Validated Feasibility Study of Integrally Stiffened Metallic Fuselage Panels for Reducing Manufacturing Costs. Boeing Commercial Airplane Group, Seattle, Washington, Report number: NASA/CR-2000-209337.
Peddieson, J., Buchanan, G., 1990. Mathematical modeling of an age-forming process. Math. Comput. Model. 14 (5), 1057–1060.
Sallah, M., Peddieson, J., Foroudastan, S., 1991. A mathematical model of autoclave age forming. J. Mater. Process. Technol. 28, 211–219.
Yang, H., 2013. Creep Age Forming Investigation on Aluminium Alloy 2219 and Related Studies. Imperial College London, PhD thesis.
Yang, H., Davies, C.M., Lin, J., Dear, J.P., 2013. Prediction and assessment of springback in typical creep age forming tools. Proc. Inst. Mech. Eng. Part B: J. Eng. Manuf. 227 (9), 1340–1348.
Zhan, L., Lin, J., Dean, T.A., Huang, M., 2011a. Experimental studies and constitutive modelling of the hardening of aluminium alloy 7055 under creep age forming conditions. Int. J. Mech. Sci. 53 (8), 595–605.
Zhan, L., Lin, J., Dean, T.A., 2011b. A review of the development of creep age forming: experimentation, modelling and applications. Int. J. Mach. Tools Manuf. 51 (1), 1–17.